RSC Advances

PAPER

View Article Online
View Journal | View Issue

Cite this: *RSC Adv.*, 2014, **4**, 51593

Control of pressure-driven components in integrated microfluidic devices using an on-chip electrostatic microvalve†

Joshua D. Tice,[a] Amit V. Desai,[a] Thomas A. Bassett,[a] Christopher A. Apblett*[bc] and Paul J. A. Kenis*[a]

Received 12th September 2014
Accepted 2nd October 2014

DOI: 10.1039/c4ra10341f

www.rsc.org/advances

Pressure-driven actuators play a critical role in many microfluidic technologies, but the ancillary equipment needed to operate pneumatic and hydraulic platforms has limited their portability. To address this issue, we created an electrostatic microvalve used to regulate pressures in hydraulic control lines. In turn, these control lines are able to actuate pressure-driven components, *e.g.*, microvalves. The electrostatic microvalve is fabricated exclusively with soft-lithographic techniques, allowing it to be directly integrated in a microfluidic chip. The electrostatic microvalve also contains a passive structural element that balances the pressure on the top and bottom sides of the actuating membrane. This feature enables the microvalve to induce pressure changes up to 20 kPa with electric potentials less than 320 V. When the microvalve is integrated into a microfluidic "pressure amplifier" circuit, the pressure output of the circuit can be tuned with the voltage applied to the microvalve. This integration allows for different types of pressure-driven components to be actuated with variable pressures, and thus eliminates the need for off-chip pressure regulation. In the example reported here, only one actuator is required to adjust the pressure of a single hydraulic line.

Introduction

Pressure-driven actuators are employed in a number of microsystem components, including artificial muscles for soft robots,[1,2] dynamic "rails" for microparticle assembly,[3] transducers for Braille displays,[4] and microvalves for fluid control in microfluidic platforms.[5] Some of these actuators are hydraulic, *i.e.*, operated by fluids, and others are pneumatic, *i.e.*, operated by gases. Both types of pressure-driven actuators benefit from high power and force densities.[6] They also benefit from the soft-lithographic approaches used for their fabrication,[1,5] which enable the actuators to be integrated monolithically into elastomer-based microfluidic chips and soft machines, such as grippers.[1] However, despite their advantages, pressure-driven actuators have yet to see extensive use in portable applications. Currently, one of the biggest challenges for achieving portability is developing proper ancillaries for these systems. Operation of pressure-driven actuators typically requires an array of solenoid valves powered through an electrical wall outlet, as well as electronic controls, such as a computer. Furthermore, in situations where the actuators do not operate between binary states,[7–9] usually more than one pressure source is required, which further increases the bulkiness of the ancillary components.

To address the above issues, researchers are striving to engineer smaller and less energy intensive microactuators and to develop microfluidic strategies to regulate the pressure from a single source. As an example, Whitesides *et al.*[10] addressed 32 independent pneumatic control lines using an array of 64 Braille pins interfaced with a computer. The actuators were commercially available, energy efficient and modular in design. For each output, one Braille pin controlled incoming pressurized gas, while a second vented the pneumatic line to atmosphere. To adjust the pressure in the chip, the researchers simply controlled the time that gas was injected into an actuator. Another strategy for adjusting the pressure levels in a device involves the use of a microfluidic serial digital-to-analogue pressure converter.[11]

While Braille pins have shown impressive capabilities in a battery-operated platform, the price of the actuators (~%10 USD per actuator) could limit their scalability. Cheaper actuators that can be made with simple fabrication schemes in a parallel fashion and in high density are needed for microfluidic large scale integrated systems. A promising approach is the use of electrostatic microvalves, because they can be integrated with

[a]*Department of Chemical & Biomolecular Engineering, University of Illinois at Urbana-Champaign, Urbana, IL 61801, USA. E-mail: kenis@illinois.edu; Tel: +1 (217)265-0523*

[b]*Sandia National Laboratories, Albuquerque, NM 87185, USA. E-mail: caapble@sandia.gov; Tel: +1 (505)844-3497*

[c]*Department of Chemical & Nuclear Engineering, University of New Mexico, Albuquerque, NM 87131, USA*

† Electronic supplementary information (ESI) available: Simulations, materials and methods, and movie. See DOI: 10.1039/c4ra10341f

microfluidic designs in high density, and they are energy efficient.[12–19] To date, however, using these electrostatic valves to control pressure has been difficult. Others have reported a pneumatic manifold composed of electrostatic microvalves in which each pneumatic line is also controlled by two actuators,[16] similar to the aforementioned approach based on Braille pins.[10] While the electrostatic microvalves were capable of controlling pressures up to 50 kPa using electrical potentials between 200–800 V, their fabrication was rather involved, as it included the use of laser ablation and vacuum deposition. Also, when the valves were activated repetitively, the potential needed for actuation increased rapidly due to dielectric charging. The potential drift rendered the valve inoperable in as little as 20 cycles.

Previously, we reported an electrostatic microvalve for controlling pressure-driven components in portable microfluidic systems.[12] The distinguishing feature of our work was the choice of materials for the valve – poly(dimethyl siloxane) (PDMS) and carbon nanotubes – which allowed for fabrication of the valve with solely soft-lithographic techniques and it enabled seamless integration of the valve with standard hydraulic components. Additionally, by constructing all the contact surfaces out of PDMS, we avoided dielectric charging and thus drift in the actuation potential. Unfortunately, the valve could accommodate a maximum back pressure of only ~4 kPa, which severely limited the scope of its application. Most pneumatic or hydraulic applications (such as those described above[1–4,20,21]) require pressures between 10–100 kPa, with some necessitating even higher pressures. Additionally, our system was designed only for binary actuators – specifically, hydraulic microvalves.

In this paper we report a microfluidic "pressure amplifier circuit" that uses an on-chip electrostatic microvalve to regulate pressures in hydraulic control lines. By integrating a pressure-balancing element in the microvalve, we are able to induce pressure changes up to 20 kPa. Furthermore, the pressure output of the circuit can be varied by adjusting the voltage applied to the microvalve, and only one actuator is required to adjust the pressure of a single hydraulic line.

Results and discussion

Design and simulation

One example of our pressure amplifier circuit is shown in Fig. 1a. The hydraulic actuator is pressurized *via* a hydraulic control channel, which is attached to a pressure source (ideally, a small portable tank of compressed air) and vented to the atmosphere. Fig. 1a depicts the hydraulic actuator as a hydraulic microvalve, although in principle this actuator could be replaced by a number of other pressure-driven components. An electrostatic microvalve is integrated into the hydraulic control channel and regulates the flow of hydraulic fluid through the channel, which subsequently adjusts the pressurization of the control channel and the activation of the hydraulic component.

The electrostatic microvalve is composed of a circular elastomeric membrane suspended above a hydraulic control channel, with electrodes composed of carbon nanotubes embedded both in the membrane and just below the microchannel (Fig. 1b). When an adequate electric potential is applied between the two electrodes, the ensuing electrostatic force pulls the membrane into contact with the floor of the channel (the valve seat), which constricts the flow of hydraulic fluid through the control channel. The minimum electric potential needed to actuate the microvalve (the actuation potential) is highly sensitive to the distance between the

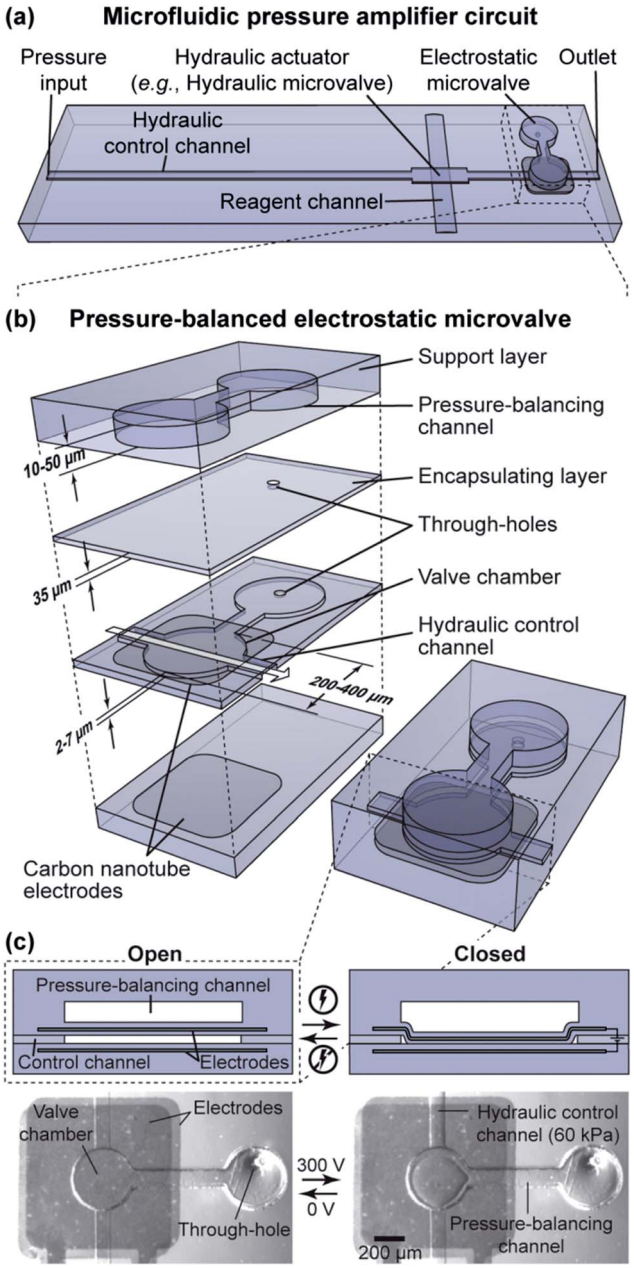

Fig. 1 Design and operation of a microfluidic pressure amplifier circuit. (a) Schematic illustration of the complete circuit. (b) Perspective view of the pressure-balanced electrostatic microvalve and its constitutive components. (c) Schematic cross-sections (side-view) and micrographs (top-view) of a pressure-balanced electrostatic microvalve in the open and closed states. All illustrations are not drawn to scale.

electrodes.[22] As such, a crucial part of the design was minimizing deflection of the microvalve's membrane away from the lower electrode as a result of pressurization of the hydraulic control line. In our previously reported design, we attempted to prevent this unwanted deflection by attaching a post to the top-side of the membrane.[12] Although finite element analysis predicted that the post decreased deflection of the membrane by a factor of about two (Fig. S1a and b; see ESI†), the membrane still deformed by ~0.5 μm kPa^{-1} in our simulations. When we experimentally tested that design with a post, electrostatic actuation allowed control of the pressure in the hydraulic control channel up to no more than ~4 kPa.[12] Thus, we decided to not pursue this approach further.

Further simulations predicted that by removing the post and balancing the hydraulic pressure on the top-side and bottom-side of the membrane, the unwanted deflection of the membrane could be minimized further as explained in detail in the ESI (Fig. S1c and d†). To implement this strategy, we integrated a peripheral microchannel that led from the microvalve chamber to a through-hole and then to a cavity above the microvalve's membrane. This feature allowed the pressure of the hydraulic fluid on both sides of the membrane to equalize dynamically *via* passive fluidic communication (Fig. 1b and 2a). With this modification in place, our simulations predicted that the center of the membrane would deflect vertically less than 0.01 μm kPa^{-1} (Fig. 2b and c). In fact, the floor of the microvalve chamber deflected more than the membrane (0.04 μm kPa^{-1}). Incorporating a second pressure balancing feature on the other side is possible, but not necessary. The design we settled on incorporates a single pressure-balancing channel.

Our microfluidic pressure amplifier circuits – composed of the electrostatic microvalve, the hydraulic control channel, and the hydraulic actuator – were arranged to mimic rudimentary single-stage field-effect transistor (FET) amplifier topologies (Fig. 3). The hydraulic control channel can be thought of as a fluidic resistor, and the electrostatic microvalve can be envisioned as a depletion-mode junction FET, since both the microvalve and the analogous electronic component operate by constricting flow of the relevant medium – hydraulic fluid in the case of the electrostatic microvalve and charge carriers in the case of the FET (Fig. 3a and b). The pressure source serves the function of a voltage input, while the pressure of the hydraulic actuator is the output.

The position of the electrostatic microvalve along the hydraulic control channel relative to the inlet, in addition to its position relative to the hydraulic actuator, defines the operating mode of the microfluidic circuit. When the electrostatic microvalve is just upstream of the outlet and the hydraulic actuator is placed just upstream of the microvalve, we refer to the configuration as a microfluidic buffer (Fig. 3a and c), analogous to an electrical buffer. (Note that in principle this system is compatible with a variety of hydraulic actuators, but for illustrative purposes, a hydraulic microvalve is depicted in Fig. 3c.) With the electrostatic valve in the open position, hydraulic fluid is allowed to flow through the control channel, and a pressure gradient develops, as shown qualitatively in Fig. 3c. Due to its proximity to the outlet, the hydraulic actuator experiences a pressure close to atmospheric, and remains unactuated. When the electrostatic microvalve is closed, flow is restricted, which causes a buildup of pressure in the control channel upstream of the electrostatic microvalve, which subsequently activates the hydraulic actuator.

By switching the inlet and the outlet of the microfluidic pressure amplifier circuit, we change the functionality from a microfluidic buffer to a microfluidic inverter (Fig. 3b). In this case, the electrostatic microvalve is just downstream of the pressure source, and the hydraulic actuator is just downstream of the microvalve (Fig. 3d). Now, when the electrostatic microvalve is open and a pressure gradient is allowed to stabilize, the hydraulic actuator experiences the high end of the gradient and activates (Fig. 3d). Closing the electrostatic microvalve increases the fluid resistance upstream of the hydraulic actuator in the control line, causing a pressure drop that deactivates the hydraulic component.

To aid the design of the microfluidic pressure amplifier circuits, we developed a simple analytical model to predict the effect of key geometrical dimensions on the circuit's performance. Consider the microfluidic pressure amplifier circuits

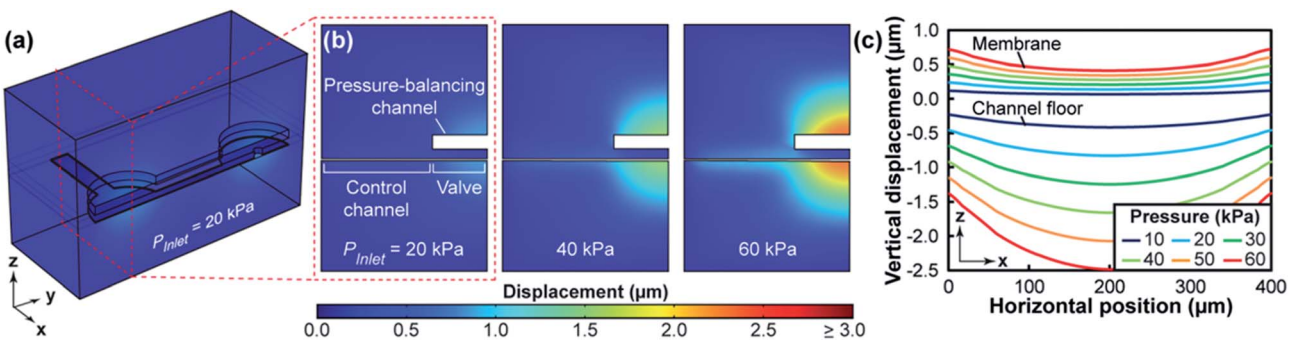

Fig. 2 Finite element analysis of an electrostatic microvalve when subjected to pressurization. (a) Cut-away of a three-dimensional model of the microvalve. The simulated pressure (P_{inlet}) was 20 kPa. (b) Cross-sections bisecting half of the microvalve chamber in the x–z plane. The pressures applied to the channels in the simulation were 20, 40, and 60 kPa, respectively, from left to right. (c) Graph of the vertical displacement of the membrane and the floor of the microvalve chamber as a function of the applied pressure. Data were derived from the x–z plane bisecting the microvalve chamber.

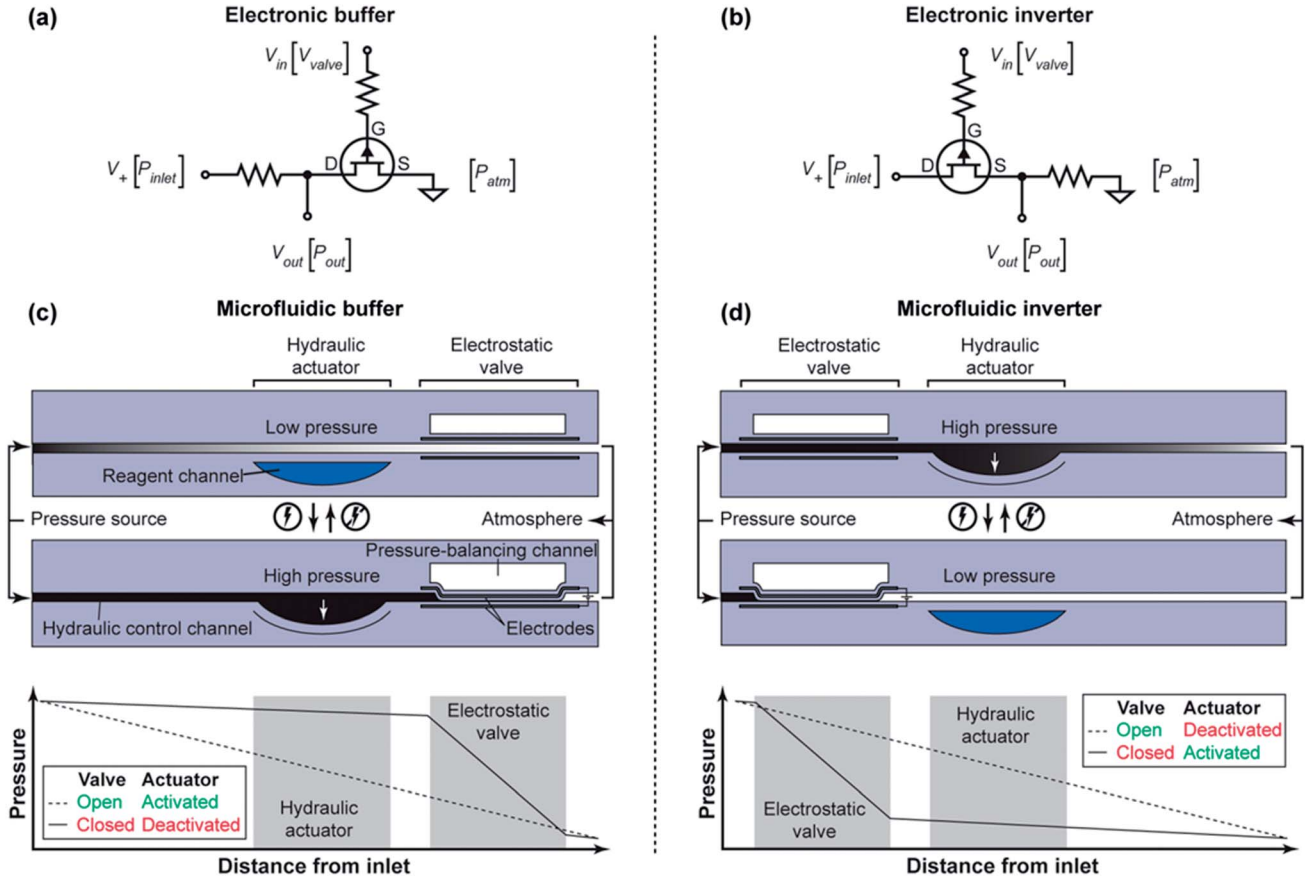

Fig. 3 Microfluidic amplifier circuits with integrated pressure-balanced electrostatic microvalves. An electric circuit diagram of (a) a single-stage field-effect transistor amplifier in a buffer configuration (D drain; G gate, and S source), and (b) an electric inverter. The common abbreviations for the electrical terminals (V_+, V_{in}, V_{out}) are shown, with the analogous microfluidic circuit equivalents (P_{inlet}, V_{valve}, P_{out}) in brackets. Illustrations of (c) a microfluidic buffer and (d) for a microfluidic inverter, each with a corresponding qualitative graph of the pressure drop in the microfluidic circuit with the electrostatic microvalve open and closed.

illustrated in Fig. 4a and c. As an approximation, we assumed a rigid channel, although the deformability of PDMS channels is well-known.[23,24] We then used a simplified form of Hagen–Poiseuille's law to approximate the pressure drop in a channel:

$$\Delta P = QR_h, \tag{1}$$

where ΔP is the pressure drop, Q is the volumetric flow rate, and R_h is the hydraulic resistance. Using a hydraulic-electric circuit analogy,[25] we expressed the pressure output of the hydraulic actuator, P_{out}, in the rest state as in eqn (2), while assuming that the electrostatic microvalve is fully open and contributing negligible fluidic resistance:

$$P_{out} = P_{inlet}\left(1 - \frac{R_{h,upstream}}{R_{h,upstream} + R_{h,downstream}}\right), \tag{2}$$

where P_{inlet} is the pressure at the inlet of the control channel, and $R_{h,upstream}$ and $R_{h,downstream}$ are the hydraulic resistances of the upstream and downstream segments of the control channel (relative to the position of the electrostatic microvalve), respectively. Since the hydraulic resistance of a rigid channel segment scales linearly with length, $L_{segment}$, eqn (2) can be simplified to:

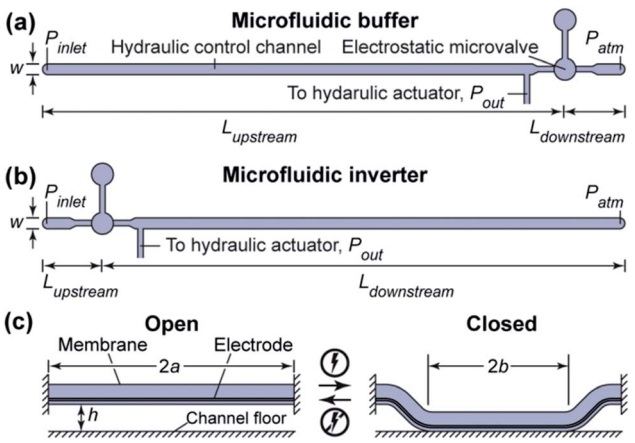

Fig. 4 Schematic illustrations of top-views of (a) a microfluidic buffer and (b) a microfluidic inverter. (c) A simplified cross-section of the membrane of the electrostatic microvalve in the open and closed state.

$$P_{out} = P_{inlet}\left(1 - \frac{L_{upstream}}{L_{upstream} + L_{downstream}}\right). \quad (3)$$

When the electrostatic microvalve is closed, typically two narrow "leakage channels" form around the periphery of the valve chamber due to the rectangular nature of the chamber's cross section (Fig. 1c). These leakage channels contribute an additional finite hydraulic resistance, $R_{h,valve}$, which then is incorporated into the expression for P_{out}, eqn (2). The expression for P_{out} for the microfluidic buffer then becomes:

$$P_{out} = P_{inlet}\left(1 - \frac{R_{h,upstream}}{R_{h,upstream} + R_{h,downstream} + R_{h,valve}}\right), \quad (4)$$

while the expression for P_{out} for the microfluidic inverter becomes:

$$P_{out} = P_{inlet}\left(1 - \frac{R_{h,upstream} + R_{h,valve}}{R_{h,upstream} + R_{h,downstream} + R_{h,valve}}\right). \quad (5)$$

When designing the microfluidic pressure amplifier circuits, we first considered eqn (3). Ideally, in the case of the microfluidic buffer, $L_{upstream}$ is much larger than $L_{downstream}$ such that P_{out} approaches P_{atm} when the electrostatic microvalve is in the rest state. Similarly, to satisfy that P_{out} approaches P_{inlet} for the microfluidic inverter in the rest state, we wanted to meet the condition $L_{upstream} \ll L_{downstream}$. Pragmatically, we set $L_{upstream} = 10 \times L_{downstream}$ for the microfluidic buffer and $L_{upstream} = 0.1 \times L_{downstream}$ for the microfluidic inverter.

In regards to the total length of the control channel, several constraints dictated that the control channel be as short as possible. Firstly, large hydraulic resistance in the control channel would impede fluid flow, decreasing the response time of a microfluidic circuit. Secondly, we had to consider the limited chip real-estate on our devices. Thirdly, from eqn (4) and (5) follows that when the electrostatic microvalve is closed the condition $R_{valve} \gg R_{h,upstream} + R_{h,downstream}$ must be met; then P_{out} approaches P_{inlet} for the microfluidic buffer, and P_{out} approaches P_{atm} for the microfluidic inverter. To keep $R_{h,upstream} + R_{h,downstream}$ as low as possible, we minimized the length of the control channel while maximizing its width, w. We set $L_{upstream} = 10$ mm, and $L_{downstream} = 1$ mm for the microfluidic buffer, and $L_{upstream} = 1$ mm, and $L_{downstream} = 10$ mm for the microfluidic inverter. We were able to make the channel as wide as 200 μm without observing unwanted collapse of the channel during fabrication.

The design of the electrostatic microvalve necessitated two main considerations. Firstly, we needed to minimize the electric potentials needed to operate the microvalve while maximizing the hydraulic pressure that could be applied. Secondly, when the electrostatic microvalve is closed, two narrow "leakage channels" form around the periphery of the valve chamber due to the rectangular nature of the chamber's cross section (Fig. 1c). We wanted to be able to tune the cross-section of these "leakage channels" such that the pressure in the microfluidic chip could be adjusted within a wide dynamic range. We also needed to be capable of attaining near-closure when needed. The ESI† contains a rough model that predicts how the pressure output of the microfluidic circuits depends on the extent of valve closure (b/a in Fig. 1c) and the height of the valve chamber (which is the same as the height of the control channel, h). However, fully developing the mathematical model to predict appropriate geometrical parameters for the electrostatic microvalve was non-trivial. The operation of the electrostatic microvalve involves highly nuanced behavior, including elastomeric deformation due to pressurization, non-uniform electric fields, surface adhesion, and time-dependent fluid flow through the valve chamber. Hence, to ascertain an appropriate geometry for the electrostatic microvalve, we interrogated a set of parameters experimentally.

Fabrication

We fabricated electrostatic microvalves and pressure amplifier circuits using only soft-lithographic techniques (Fig. 5). Detailed descriptions are provided in the ESI.† Briefly, to form the electrodes of the electrostatic microvalve (Fig. 5a), an aqueous suspension of multi-walled carbon nanotubes (MWNTs) was filtered through a hydrophilic membrane. After the solvent was removed, the resulting MWNT film was washed and dried.

To construct the upper layers of the microvalve (Fig. 5b), a thin layer of PDMS was spin-coated onto a mold such that a thin film covered the channel features. Molds were fabricated with standard photolithographic techniques. In some cases, posts were patterned on the mold, which were tall enough to protrude beyond the PDMS film, thus forming through-holes. After the PDMS film was cured, a separate PDMS stamp was brought into contact with the previously formed MWNT film. Areas in contact with the stamp were lifted off the membrane filter and then applied to the PDMS film. Pressure was applied by hand, and after lifting off the PDMS stamp, a fraction of the MWNT film transferred to the PDMS film. The transparency of the MWNT film allowed us to perform alignment in a straight-forward manner. Characterization of the transfer printing process and the optical and electrical properties of the electrodes has been reported elsewhere.[12,13,26] Electrical contacts were made from a mixture of PDMS and MWNTs. To encapsulate the MWNT electrode, a second layer of PDMS was spin-coated on top of the electrode and cured. The PDMS support layer was aligned onto the membrane, and the whole assembly was subjected to an extended heat treatment. The support layer sealed permanently to the membrane due to purposely mismatching the crosslinker-to-monomer ratio between the layers.[5] The upper layers of the microvalve were removed from the mold and holes were punched to the inlets of the microchannels. If through-holes were not formed previously by means of posts incorporated into the molds, the through-holes were cut with a scalpel or sharpened needle.

To fabricate the lower electrode for the microvalve (Fig. 5c), a thin layer of PDMS diluted with hexanes was first spin-coated onto a plain wafer. The thin PDMS layer was cured, and then a MWNT film was applied as described above. Electrical

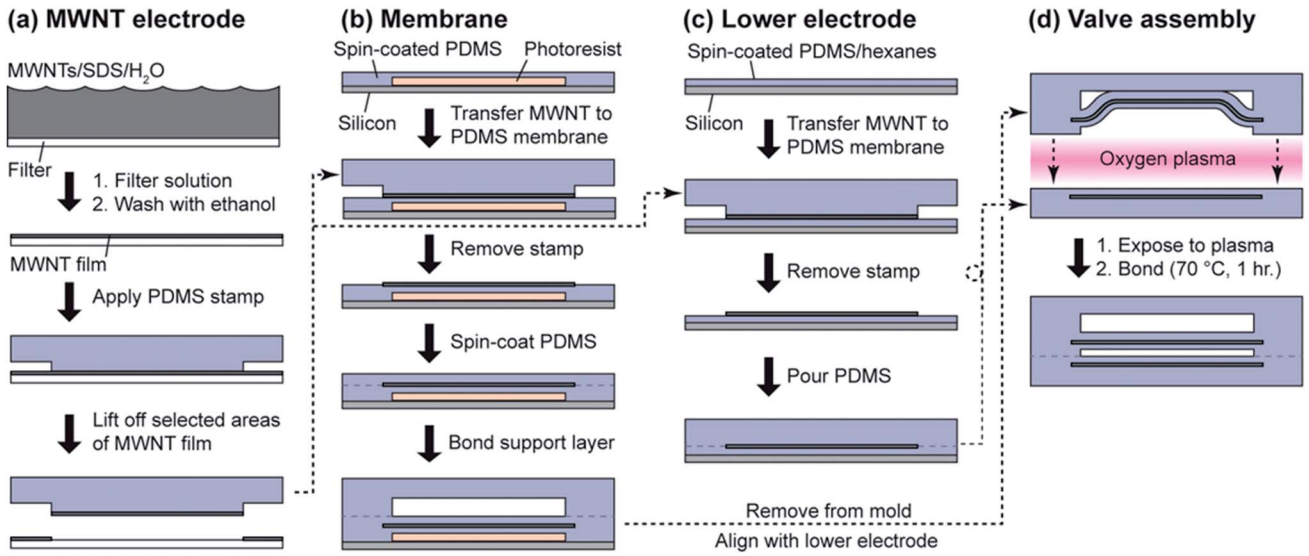

Fig. 5 A flow diagram of the soft-lithographic method used to fabricate the pressure-balanced electrostatic microvalves.

contacts were also applied, and the wafer was then covered with a layer of PDMS several millimeters thick, which was cured with a heat treatment.

Hydraulic actuators could be integrated into either the upper or lower layers of the device. Details of both approaches are included in the ESI.† To seal the upper layers of the microvalve to the lower electrode (Fig. 5d), both surfaces participating in the seal were exposed to oxygen plasma and then brought into contact. During the sealing process, the membrane was reversibly laminated to the top of the pressure-balancing channel to prevent unwanted collapse of the membrane onto the floor of the microvalve chamber. After the bond was completed, the membrane was delaminated by pressurizing the channels.

Characterization of actuation potentials and back pressures of the electrostatic microvalve

With our earlier design,[22] electrostatic microvalves with posts that had a membrane thickness of 35 μm, a diameter between 200–400 μm, and a height between 2–7 μm were able to actuate with potentials < 320 V and were also able to re-open when the electric potential was turned off (*i.e.*, the restoring force of the membrane was able to overcome surface adhesion between the membrane and the channel floor). To identify effective dimensions for the present design, we started by quantifying the operational limits of the microvalve within this design space, specifically (i) the pressures that could be applied to the hydraulic control channel while still permitting actuation potentials ≤ 320 V and (ii) the pressures that the microvalves could withstand in the closed state without re-opening, also with potentials ≤ 320 V. We refer to the microvalve as "open" when the membrane is not in contact with the channel floor and "closed" when the membrane is in contact (Fig. 1c). We chose an upper limit of 320 V because in some cases the high electric fields generated with potentials above this limit led to electrical breakdown of the membrane. This limit also ensured that the valves would be compatible with a portable electric controller we had built previously.[13]

First, we determined actuation potentials by holding the inlet pressure constant and then gradually increasing the electric potential until the membrane snapped shut against the floor of the actuator chamber (Path 1 → 2 in Fig. 6a). The actuation potential increased linearly with applied pressure over the range of pressures tested (Fig. 6b1 and c1). The actuation potential also increased with increasing gap size and decreased with increasing diameter, as predicted in a previous modeling study.[22] With the largest tested diameter of 400 μm and the shallowest gap of 2 μm, the microvalves actuated with applied pressures up to 62 kPa using an actuation potential of 302 ± 18 V. Note that this pressure was more than twelve times the pressure that could be accommodated by the design we reported earlier.[12]

After the microvalve was closed, we gradually increased the pressure of the fluidic control line to determine the maximum pressure that could be applied without reopening the microvalve (Path 3 → 4 in Fig. 6a). The threshold pressures increased linearly with electric potential. They also increased with increasing diameter, and remained similar with respect to the gap between the electrodes. Microvalves with shallow channel heights of 2 μm, 400 μm diameter and applied potential of 300 V still had the membrane in contact with the valve seat up to 150 kPa, a ten-fold improvement over the design we reported previously.[12] These data, along with the results discussed in the previous paragraph, show that the pressure-balancing scheme substantially increases the back pressure that the electrostatic microvalve can accommodate. With the pressure-balancing channel in place, the electrostatic microvalve was able to operate with relevant pressures for hydraulic microfluidic systems.

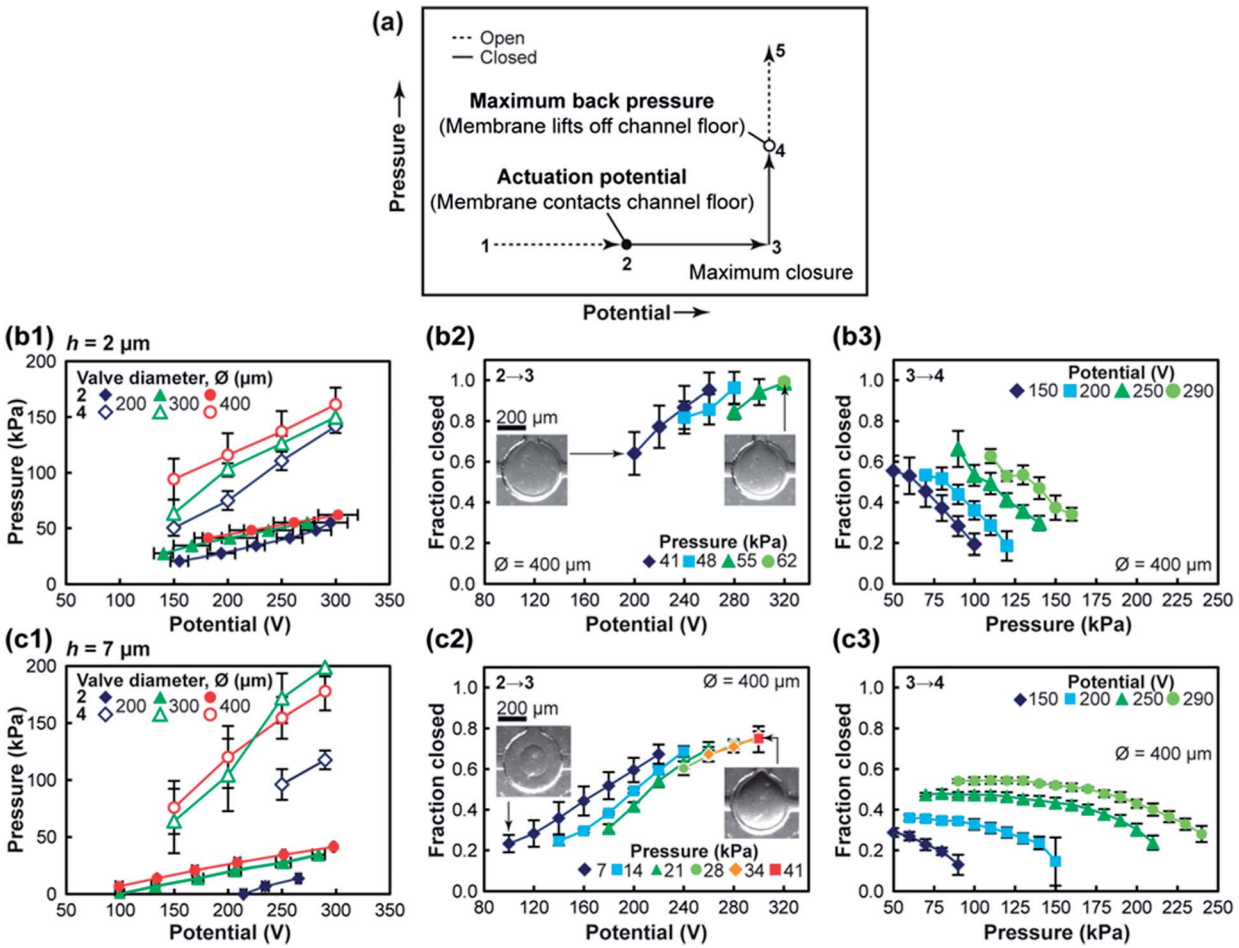

Fig. 6 Characterization of the actuation of pressure-balanced electrostatic microvalves when subjected to pressurization. (a) Graphic representation of a test cycle. (b1) Graph of the threshold potentials needed to close (*i.e.*, establish initial contact between the membrane and the channel floor) electrostatic microvalves at fixed pressures (solid symbols), and the threshold pressures needed to re-open the microvalves at fixed potentials (open symbols). The initial gap between the membrane and the channel floor was 2 μm. (b2 and b3) Graphs showing the fraction of the area of an electrostatic microvalve's membrane in contact with the channel floor as a function of (b2) electric potential (at constant pressure) and (b3) pressure (at constant potential). The initial gap was 2 μm. In (b1) micrographs of a top-view of the valve chamber are shown. (c1–c3) Same as (b1–b3), respectively, only the initial gap was 7 μm. Error bars indicate one standard deviation. h = initial gap between membrane and channel floor in unpressurized state. Ø = microvalve diameter.

Characterization of the extent of valve closure as a function of pressure and voltage

Next we sought to verify that the valves could attain a high extent of closure. We characterized the fraction of the membrane area in contact with the valve seat as a function of V_{valve} using an electrostatic microvalve with a diameter of 400 μm, since this dimension accommodated the highest back pressure in the previous section. We held the pressure of the control channel constant and then gradually increased the electric potential of the electrostatic microvalve, V_{valve}, while taking micrographs to measure the fraction of the membrane's area in contact with the valve seat (Fig. 6a2 and b2). When the height of the valve chamber, h, was 2 μm, one or both of the peripheral leakage channels collapsed to form a hermetic seal at high potentials. We found that we could accomplish nearly complete valve closure for pressures up to 62 kPa while keeping $V_{valve} \leq 320$ V (Fig. 6b2). When the height of the valve chamber was 7 μm, the maximum extent of valve closure was less than above (Fig. 6c2). However, we could access a wider range of valve closure (between 20–80%) with this height.

To simulate the build-up of pressure that was intended to occur during the course of operation of a microfluidic pressure amplifier circuit, we also interrogated the fraction of the membrane touching the valve seat when the valve was shut and the pressure was systematically increased, with constant V_{valve} (Path 3 → 4 in Fig. 6a). Again, we took micrographs at various stages of the pressurization process to quantify the fraction of the membrane in contact with the valve seat. At low pressures, the fraction of the membrane in contact with the valve seat fluctuated erratically when the height of the microvalve chamber was 2 μm, so no data are reported. At higher pressures, the membrane delaminated in a stable manner, and a linear dependence became apparent (Fig. 6b3). From these data, a rate of delamination of 5–6% of the area of the membrane per kPa

was determined. As expected, higher values of V_{valve} increased the ability of the microvalve to remain shut. Extrapolating from the trends in Fig. 6b3, we approximated that the valves could retain 80% closure with back pressures up to ~70 kPa.

When the height of the microvalve chamber was 7 μm, the membrane delaminated stably over a wider range of pressures than in the case where the height of the valve chamber was 2 μm (Fig. 6c3). However, considering the higher actuation potentials needed for the $h = 7$ valve configuration and the lower degree of closure attainable with this configuration, we concluded using valves with $h = 2$ μm would yield more suitable pressure amplifier circuits.

Characterization of pressure output of microfluidic pressure amplifier circuits

Having identified geometrical parameters suitable for the pressure-balanced electrostatic microvalve, we integrated the microvalves into complete microfluidic pressure amplifier circuits for testing. To experimentally ascertain the pressures that could be generated by the microfluidic circuits (P_{out}), we incorporated a microfluidic pressure sensor into the circuits, which consisted of a membrane suspended above a circular fluidic chamber attached to the control channel (Fig. 7a). Pressurization of the fluidic chamber caused the membrane to flex, and reference marks were patterned into the membrane, allowing the degree of flexing to be quantified and calibrated (Fig. 7b). Depending on using this configuration as a microfluidic buffer or a microfluidic inverter, the pressure sensor ended up being just upstream or just downstream of the electrostatic valve because the direction of flow was opposite for the buffer and inverter (Fig. 7a). The pressures were measured as a function of the inlet pressure (P_{inlet}) and the electric potential applied to the electrostatic microvalves (V_{valve}). In the microfluidic buffer, increasing the electric potential from 0 V to 300 V caused the pressure measured by the sensor to increase by approximately 20 kPa for all inlet pressures tested (60, 80, and 100 kPa) (Fig. 7c). In the microfluidic inverter, increasing the electric potential from 0 V to 300 V caused the pressure measured by the sensor to decrease between 10–20 kPa. The highest pressure output of the buffer was ~95 kPa, achieved at V_{valve} of 300 V and a P_{inlet} of 100 kPa.

Interestingly, the pressures we could access with the pressure amplifier circuits were higher than the limits we expected from the earlier characterization depicted in Fig. 6. The major difference between the two sets of experiments was that fluid flow was established in the hydraulic control line of the pressure amplifier circuits (Fig. 7), whereas the hydraulic fluid was static in the valve characterization studies (Fig. 6). We postulate that the presence of a pressure gradient enhanced the operation of the electrostatic microvalve. When the microvalve was open, non-uniform pressure in the valve chamber may have led to an advantageous distortion of the membrane such that the distance between electrodes was decreased in certain areas, increasing the local strength of the electric field. In fact, in certain cases we observed that the membrane partially touched the valve seat when the electrical potential was removed from

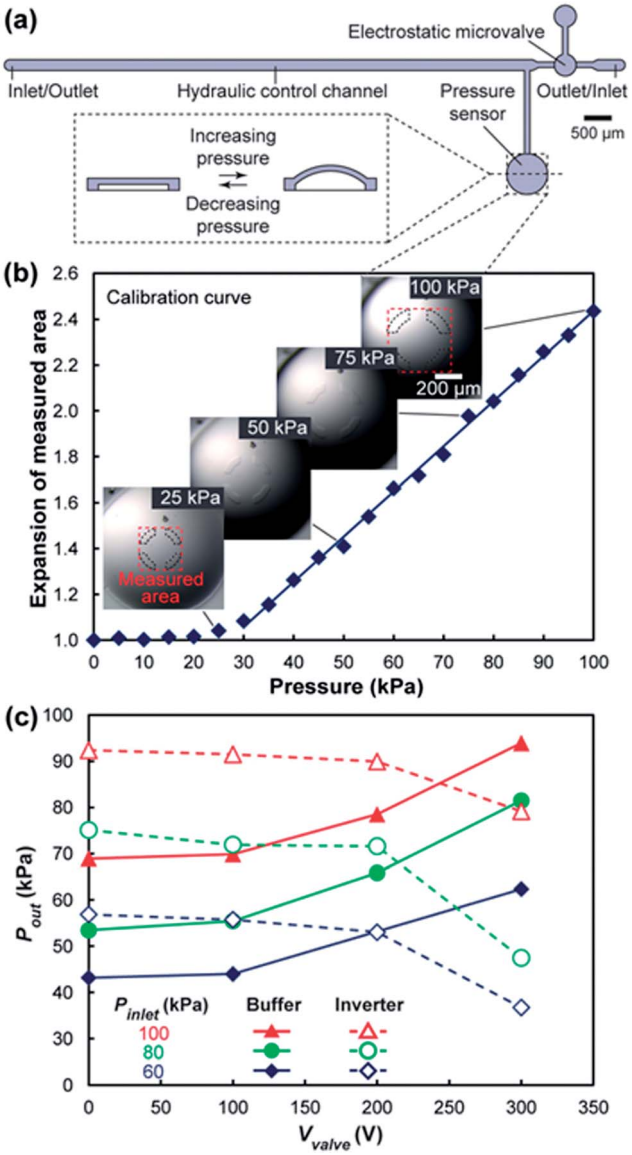

Fig. 7 Measurement of the pressure output of microfluidic pressure amplifier circuits. (a) Top-down view, drawn to scale, of a test device with an integrated membrane-based pressure sensor. (b) Micrographs of the pressure sensor's response to several levels of pressure, and a calibration curve showing the expansion of the measured area in response to pressurization. (d) A graph illustrating the pressure output (P_{out}) of microfluidic buffers and inverters for multiple values of potential (V_{valve}) and input pressure (P_{inlet}).

the electrostatic microvalve (Movie S1†). This could in principle also be partially due to other phenomena, such as dielectric charging, although we believe dielectric charging is not occurring in the system studied here.[12] With the valve closed, we observed that the leakage channels were wide on the high-pressure side of the valve chamber, but formed "pinch-points" on the downstream side of the valve chamber where the pressure was lower. These pinch-points typically constricted to only a few microns in width. Qualitatively, they also appeared to be more stable in width than the leakage channels in the valve characterization studies.

In Fig. 7c, P_{out} for the microfluidic buffer in the rest state was higher than predicted by our model in eqn (3). Ideally, P_{out} would be less than 10% of P_{inlet} in this case. We investigated whether the discrepancy was due to unexpected hydraulic resistance downstream of the sensor. However, simulations showed that the pressure drop due to the rapid expansion from the control channel to the outlet access hole was expected to be negligible (simulations not shown). Also, we calculated the hydrostatic pressure of fluid in the outlet and found that to be negligible as well. Another more likely explanation for our observation could be a lower value of hydraulic resistance upstream of the sensor compared to the resistance predicted by our rudimentary model. We knowingly made the assumption that the control channel was rigid to simplify our analysis. However, judging by the theoretical and experimental work done by us[23] and others,[24] we would expect the cross-section of the control channel to expand significantly due to pressurization, which would have the effect of decreasing the hydraulic resistance of the control channel, especially upstream of the sensor, where pressure was greatest. More elaborate models incorporating the elasticity of PDMS could be used to design microfluidic pressure amplifier circuits with predictable P_{out} when $V_{valve} = 0$ V.

The data in Fig. 7c showcase a major advantage of our system in that it can dynamically access a range of output pressures merely by adjusting V_{valve}. As alluded to previously, thus far, most pneumatic or hydraulic control schemes have been tailored for binary state actuators, such as microvalves,[20] Braille displays,[4] or rails.[3,4] However, applications that incorporate actuators with more than two states (*e.g.*, high-radix multiplexers[7]), or non-discretized states (*e.g.*, tunable lenses,[8,9] similar in construction to the pressure sensor depicted in Fig. 7a and b, or soft robots[1,2]) typically require multiple pressure inputs or external regulators. With the microfluidic circuits reported here, only a single pressure input was required, and the pressure was adjusted on-chip.

Control of a hydraulic microvalve with a microfluidic pressure amplifier circuit

Considering the prevalence of hydraulic microvalves in a broad range of microfluidic applications, we conducted a proof-of-principle where a microfluidic buffer was utilized to activate a single hydraulic microvalve (Fig. 8). The dimensions of the hydraulic microvalve were chosen such that the pressure required for hermetic closure was 80–90 kPa,[27] and P_{inlet} was set to 100 kPa. The diameter of the electrostatic microvalve was 400 μm, and h was set to 2 μm, the optimal dimensions we determined above. With the electrostatic microvalve in the rest state, the membrane of the hydraulic microvalve deflected slightly due to the pressure gradient in the control channel, although a continuous fluid path was clearly visible in the reagent channel of the hydraulic microvalve (Fig. 8a). When 250 V or more was applied to the electrostatic microvalve, the membrane of the hydraulic microvalve deflected further and formed a hermetic seal in the reagent channel (Fig. 8b). Releasing the potential returned both the electrostatic and the hydraulic microvalve to their original states. See Movie S1 in the ESI† for clear visualization of the membrane of the electrostatic microvalve contacting the valve seat and subsequent activation of the hydraulic microvalve.

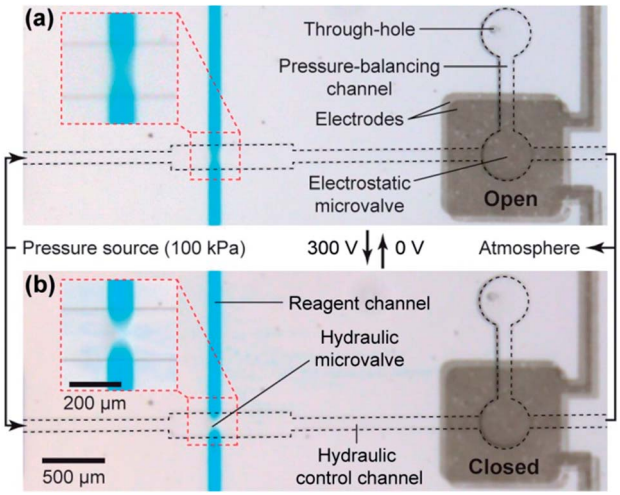

Fig. 8 Micrographs of a microfluidic buffer with an integrated hydraulic microvalve where the hydraulic microvalve is (a) open and (b) closed.

We also tested the frequency response of the microfluidic circuit, as certain applications require rapid, extended cycling of microvalves, *e.g.*, peristaltic pumping.[5] A square-wave signal with peak-to-peak voltage of 250 V was applied to the microfluidic buffer, and we cycled the microvalve up to 5 Hz. Above this frequency the electrostatic actuator essentially remained open due to the timescale needed for the release of the membrane from the floor of the channel. This experiment shows that peristaltic pumping is possible, with a limit in the actuation frequency of 5 Hz.

Touch-mode electrostatic actuators commonly face the issue of drift in actuation potential due to a build-up of charge on the surfaces of electrodes.[28] Either actuation potentials become prohibitively high, or the elements of the actuator fuse together, preventing further operation. We cycled our electrostatic microvalve continuously more than 2000 times without observing these common failure modes, which we believe is due to the material symmetry between the membrane and the lower electrode.[12] Instead, operation of the electrostatic microvalve was eventually inhibited by a loss of conductivity between the electrical controls and the electrical components of the microfluidic amplifier circuit. Once the connection was reset, the microvalve was able to actuate more than 2000 times again before the same failure mechanism occurred. We hypothesize that the small cross-sectional area of contact between electrical controls and the microfluidic device induced high current fluxes at the interface, which gradually burned out the connection. This issue could probably overcome in future designs by using connections with larger cross-sectional interfaces, perhaps in conjunction with liquid metals to mediate contact between the conductive polymers and electrical wiring.[29]

Conclusions

In conclusion, we have developed a pressure-balanced electrostatic microvalve that is highly suitable for large scale microfluidic platforms with pressure-driven actuators. Because the electrostatic microvalves are of the same length scale as common hydraulic actuators, they have the potential to scale well in these systems.

While we demonstrated a parallel instruction approach with one pressure amplifier circuit controlling a single hydraulic microvalve, in principle, many hydraulic microvalves could be controlled with a single electrostatic valve. Also, the electrostatic microvalves may significantly benefit serial instruction schemes when combined with cascading pneumatic logic structures. For instance, serial instruction typically requires a clocking and triggering signal. With the electrostatic microvalve reported here these signals can be controlled directly on-chip, thus eliminating the need for the typically used external solenoid valves.

The pressure-amplifier circuits also simplify world-to-chip connections. With electrostatic microvalves integrated on-chip, only one pneumatic connection is required, and with further development, electrical interconnections could eventually be standardized. Finally, while the current design of the electrostatic microvalve can induce pressure changes up to 20 kPa and can accommodate back pressures up to ~100 kPa with electric potentials $\leq$ 300 V, we believe further design improvements (*e.g.*, incorporation of stiffer materials) could easily improve the current operational limits, for example resulting in larger dynamic ranges and higher pressure outputs, which in turn will broaden the utility of this on-chip pressure control technology.

Acknowledgements

We thank Dr Gregory Ten Eyck, Andrew Collard, and Christopher Hamlin for assisting with preliminary fabrication and characterization. Dr James Wentz and John Roschek generously provided electrical testing equipment; Dane Sievers assisted in the measurement of sheet resistance of MWNT films, and Li Gao measured the cross-sectional dimensions of the microvalve. We also gratefully acknowledge financial support from Sandia National Laboratories, funded by the DOE through grant LDRD PR#922327; the Center for Nanoscale Chemical Electrical Mechanical Manufacturing Systems (Nano-CEMMS) at the University of Illinois, funded by the NSF through grant DMI-0328162; and the Center for Microanalysis of Materials in the Frederick Seitz Materials Research Laboratory Central Facilities at the University of Illinois.

Notes and references

1 F. Ilievski, A. D. Mazzeo, R. F. Shepherd, X. Chen and G. M. Whitesides, *Angew. Chem.*, 2011, **123**, 1930–1935.
2 R. F. Shepherd, F. Ilievski, W. Choi, S. A. Morin, A. A. Stokes, A. D. Mazzeo, X. Chen, M. Wang and G. M. Whitesides, *Proc. Natl. Acad. Sci. U. S. A.*, 2011, **108**, 20400–20403.
3 S. E. Chung, W. Park, S. Shin, S. A. Lee and S. Kwon, *Nat. Mater.*, 2008, **7**, 581–587.
4 W. Xiaosong, K. Seong-Hyok, Z. Haihong, J. Chang-Hyeon and M. G. Allen, *J. Microelectromech. Syst.*, 2012, **21**, 908–916.
5 M. A. Unger, H. P. Chou, T. Thorsen, A. Scherer and S. R. Quake, *Science*, 2000, **288**, 113–116.
6 M. De Volder and D. Reynaerts, *J. Micromech. Microeng.*, 2010, **20**, 043001.
7 D. W. Lee and Y.-H. Cho, *Lab Chip*, 2009, **9**, 1681–1686.
8 N. Chronis, G. Liu, K.-H. Jeong and L. Lee, *Opt. Express*, 2003, **11**, 2370–2378.
9 J. Chen, W. Wang, J. Fang and K. Varahramyan, *J. Micromech. Microeng.*, 2004, **14**, 675.
10 B. Mosadegh, A. D. Mazzeo, R. F. Shepherd, S. A. Morin, U. Gupta, I. Z. Sani, D. Lai, S. Takayama and G. M. Whitesides, *Lab Chip*, 2014, **14**, 189–199.
11 F. Yu, M. A. Horowitz and S. R. Quake, *Lab Chip*, 2013, **13**, 1911–1918.
12 J. D. Tice, T. A. Bassett, A. V. Desai, C. A. Apblett and P. J. A. Kenis, *Sens. Actuators, A*, 2013, **196**, 22–29.
13 J. D. Tice, J. B. Rosheck, C. D. Hamlin, C. A. Apblett and P. J. A. Kenis, *J. Microelectromech. Syst.*, 2013, **22**, 1251–1253.
14 T. Bansal, M. P. Chang and M. M. Maharbiz, *Lab Chip*, 2007, **7**, 164–166.
15 M. P. Chang and M. M. Maharbiz, *Lab Chip*, 2009, **9**, 1274–1281.
16 A. Douglas, A. L. Gregory and K. G. Bruce, *J. Micromech. Microeng.*, 2012, **22**, 025019.
17 E. Yildirim and H. Kulah, *J. Micromech. Microeng.*, 2011, **21**, 105009.
18 Q. Zhang, N. Pekas and D. Juncker, *Adv. Mater. Res.*, 2009, **74**, 179–182.
19 E. Yıldırım, M. A. S. Arıkan and H. Külah, *Sens. Actuators, A*, 2012, **181**, 81–86.
20 J. Melin and S. R. Quake, *Annu. Rev. Biophys. Biomol. Struct.*, 2007, **36**, 213–231.
21 W. Gu, X. Zhu, N. Futai, B. S. Cho and S. Takayama, *Proc. Natl. Acad. Sci. U. S. A.*, 2004, **101**, 15861–15866.
22 A. V. Desai, J. D. Tice, C. A. Apblett and P. J. A. Kenis, *Lab Chip*, 2012, **12**, 1078–1088.
23 S. L. Perry, J. J. L. Higdon and P. J. A. Kenis, *Lab Chip*, 2010, **10**, 3112–3124.
24 T. Gervais, J. El-Ali, A. Gunther and K. F. Jensen, *Lab Chip*, 2006, **6**, 500–507.
25 K. W. Oh, K. Lee, B. Ahn and E. P. Furlani, *Lab Chip*, 2012, **12**, 515–545.
26 J. Salzbrenner, C. Apblett and T. Khraishi, *Polym. Int.*, 2013, **62**, 608–615.
27 V. Studer, G. Hang, A. Pandolfi, M. Ortiz, W. F. Anderson and S. R. Quake, *J. Appl. Phys.*, 2004, **95**, 393–398.
28 C. Cabuz, E. I. Cabuz, T. R. Ohnstein, J. Neus and R. Maboudian, *Sens. Actuators, A*, 2000, **79**, 245–250.
29 H. Huan and L. Chang, *Characterizations and optimization of electrical contact between nanocomposite elastomer and metal*, Denver, Colorado, 2009.

